Slow-light dynamics of large-bandwidth pulses in warm rubidium vapor

Mark Bashkansky,[1,*] Guy Beadie,[1] Zachary Dutton,[2] Fredrik K. Fatemi,[1] John Reintjes,[1] and Michael Steiner[2]
[1]*Optical Sciences Division, Code 5614, Naval Research Laboratory, Washington, D.C. 20375, USA*
[2]*Radar Division, Code 5312, Naval Research Laboratory, Washington, D.C. 20375, USA*
(Received 16 May 2005; published 20 September 2005)

We study slow-light propagation dynamics in warm Rb vapor. We present data showing significant pulse reshaping when the bandwidth of the pulses is increased and present a model that qualitatively explains the observed behavior. Our data and modeling emphasize how the Doppler broadening in a warm vapor strongly affects the propagation of high-frequency components and leads to unintuitive features on the transmitted pulse shapes. This has important consequences for applications involving the delay of large-bandwidth pulses.

DOI: 10.1103/PhysRevA.72.033819 PACS number(s): 42.50.Gy

I. INTRODUCTION

Slowing of light pulses using resonant coherent interactions in atomic vapors has been demonstrated recently by several groups [1–4]. In most slow-light experiments the effect is demonstrated by delaying light pulses, in which the delays are experimentally measurable but are only a small fraction of the original pulse width. From an applications standpoint, real interest lies in demonstrating delays approaching and exceeding the probe laser pulse width [5]. It is well known that electromagnetically induced transparency (EIT) [6,7], the mechanism responsible for the slow-light, has a region of linear dispersion of finite bandwidth, usually a fraction of the Rabi splitting of the atomic levels. As the pulse bandwidth is extended beyond this linear region, it is expected to experience nonlinear dispersion and losses that lead to pulse distortion. For applications that will require maximum use of the available bandwidth within an EIT medium, understanding slow-light behavior in this transition region becomes critical for evaluating the performance parameters of potential devices.

This work is focused on the measurements and theory of pulse propagation through a gas of ^{87}Rb atoms, as the bandwidth is increased beyond the linear EIT region. The transient response of slow light has been investigated both experimentally and theoretically for cold atomic vapor in a magneto-optic trap [8]. However, our results on warm gases lead us to emphasize the importance of including Doppler shifts in the transition energies. The Doppler shifts result in significantly narrower EIT windows, yet lower overall losses for high-frequency components of pulse bandwidths. Only by including these effects can the experimental results be reproduced.

II. EXPERIMENT

Figure 1 shows (a) the schematic diagram of our experiment and (b) the simplified level structure for the ^{87}Rb D_1 transition. In this figure ν_E and ν_P represent the frequencies of the strong control field and weak probe beams, respectively. States $|0\rangle$ and $|2\rangle$ are ground states ($F=1$ and $F=2$ hyperfine levels, respectively), separated in frequency by $\Delta=6835$ MHz, and $|1\rangle$ is the excited state $F'=2$. The Doppler shift ν_D shifts the excited state with respect to laser field frequencies and is of the order of 300 MHz for our parameters. Frequency detunings from resonance (in the absence of Doppler broadening) for the control and probe beams are given by Δ_E and Δ_P, respectively. The laser is locked to a ^{87}Rb D_1 transition in the center of its Doppler profile using saturated absorption. An electro-optic modulator (EOM), driven by a pulsed rf signal, is used to produce collinear cw control and pulsed probe beams. The efficiency of the EOM is low ($\sim 1\%$) so that the control laser power stays mostly constant. The output of the EOM consists of the original laser frequency and two sidebands. To detect only the correct sideband a portion of the control beam is shifted in frequency by 80 MHz and is used as a local oscillator for heterodyne detection of the probe pulse after it goes through the Rb cell. The 1-mm-diam control and probe beams have the same circular polarization, with intensities at the cell of 30 mW/cm^2 and 0.3 mW/cm^2, respectively. The heterodyne signal corresponding to the probe beam is demodulated, and 512 pulse traces are averaged on the oscilloscope and stored on the computer.

The signal from the other EOM sideband is also demodulated and stored as a reference. The 7.5-cm-long ^{87}Rb cell is magnetically shielded and contains 30 torr of Ne as a buffer gas. Its temperature is held at 65 °C.

Figure 2 shows averaged traces of the reference and of the probe pulses after passage through the Rb cell. The experiment was performed for Gaussian (top) and near-square (bottom) shape pulses. As expected, the reference (solid) pulses propagate through the cell without any change. For the signal (dashed) pulse, the Gaussian pulse shape changes little, while the square pulse shape undergoes striking distortions. The slowed pulses are attenuated by more than two orders of magnitude. In other experiments we have observed reduced attenuation, accompanied by shorter delays, when the buffer gas is not present. For the incident square pulse, the transmitted pulse retains sharp features as the pulse turns off, indicating that high-frequency Fourier components are not completely absorbed. We have observed this "charging and

*FAX: (202) 404-8114. Electronic address: bashkansky@nrl.navy.mil

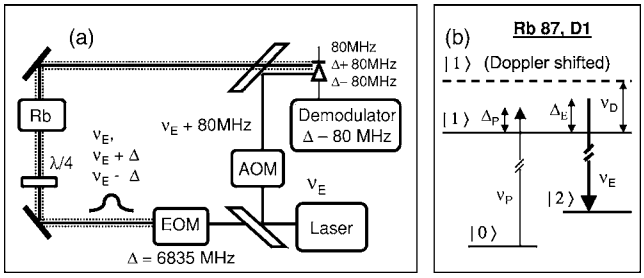

FIG. 1. (a) Experimental setup for the generation and detection of slow-light pulses. (b) Atomic-level diagram.

discharging" pulse behavior with a relatively sharp knee for various duration square pulses with and without buffer gas present. We approximate the delay through the cell to be 10 μs based on the center of the pulses. This corresponds to a group velocity of 7.5 km/s.

III. THEORY

As a starting point for our analysis, we consider an EIT model for the three-level system shown in Fig. 1(b). This well-known model calculates the EIT susceptibility using density matrix formalism in the cw regime [2]. In particular, we note that since the velocity-induced energy shifts are greater than the intrinsic linewidth, a proper calculation must include an ensemble average over the Doppler-shifted atoms. Here we examine the effect of various specific Doppler shifts and then perform the weighted average over all velocities to obtain a transmitted pulse. Only by including the Doppler shifts in the model were the simulations able to match the experimental data. From this point on angular frequency is implied for all frequency-dependent quantities, including detunings Δ_P and Δ_E.

Our equation for the EIT susceptibility, including detuning of both the probe and control frequencies, Δ_P and Δ_E, respectively, is given by

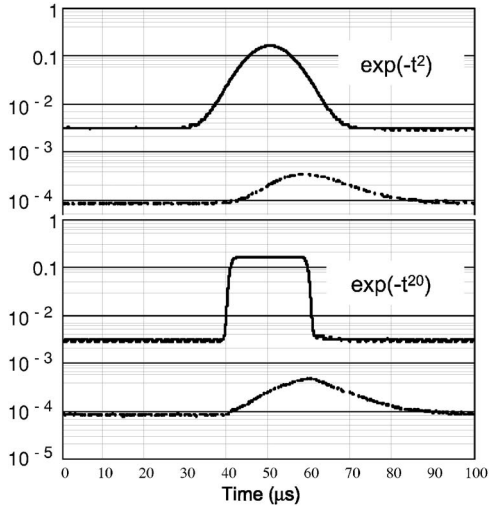

FIG. 2. Measured reference (solid) and signal (dashed) pulses after the Rb cell for Gaussian and square inputs plotted on a logarithmic scale.

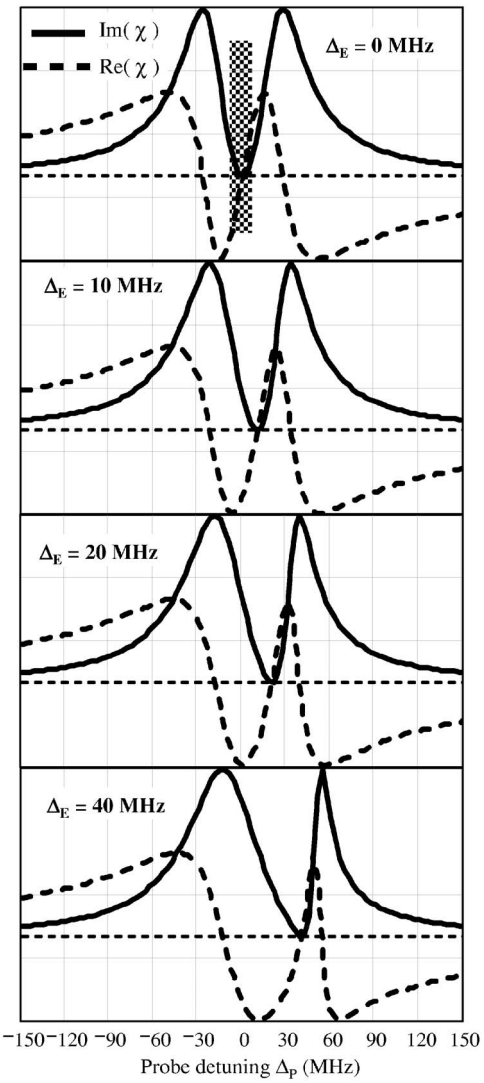

FIG. 3. Calculated susceptibility as a function of the probe angular frequency for different control field detunings Δ_E. The shaded region for Δ_E=0 represents the standard operating region for EIT: small Im(χ) (low loss) and steep, linear slope in Re(χ) (low group velocity).

$$\chi(\Delta_P, \Delta_E, \omega_D) = \frac{N\mu^2}{\varepsilon_o \hbar} \frac{4[(\Delta_P - \Delta_E) + i\gamma_{20}]}{[|\Omega_E|^2 - 4[(\Delta_P - \Delta_E) + i\gamma_{20}](\Delta_P + \omega_D + i\gamma_{10})]}. \quad (1)$$

Here N is the number of atoms per unit volume, Ω_E is the Rabi frequency of the control laser, μ is the dipole matrix element between states $|0\rangle$ and $|1\rangle$, γ_{10} and γ_{20} represent dephasing rates between the appropriate states, and ω_D the Doppler shift. The numerical values are taken from Ref. [9]. Most values, including 7.5 cm length of the cell and optical beam properties, correspond to the experimental parameters described earlier in the paper. The values used in the model included an oscillator strength of 0.23 and spatially uniform pump intensity of 30 mW/cm^2, giving a Rabi frequency Ω_E=54 MHz. We used the number density of ^{87}Rb as an

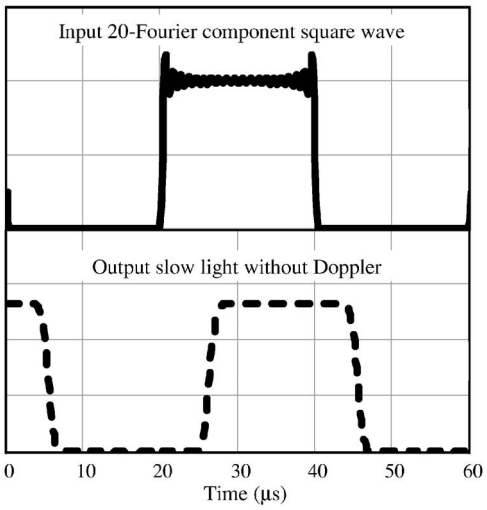

FIG. 4. Canonical slow-light behavior for a simple, zero-velocity three-level system. Higher frequencies (the ripples) are attenuated in the transmitted wave form, while the overall pulse shape is delayed with respect to the input pulse.

adjustable parameter for a better fit with the experimental results choosing $N=7.4\times10^{10}$ cm^{-3}. Our simple model does not take into consideration the nonuniform beam profile, absorption of the control laser in the cell, nonzero magnetic fields due to imperfect shielding, the presence of other atomic levels, or effects of nonuniform distribution among the various Zeeman sublevels. Due to the presence of the buffer gas, we assumed the reduced dephasing linewidth $\gamma_{20}=10^{-6}\gamma_{10}$. Our results on the pulse reshaping effects are not sensitive to the exact values of γ_{20} for small γ_{20}. Note that because we have not included any detailed modeling of these various causes of pulse attenuation in our model, our theoretical results do not address the observed pulse attenuation in Fig. 2.

We consider first the case of no Doppler broadening $\omega_D=0$, analogous to an experiment in cold Rb atoms such as those trapped in a magneto-optic trap (MOT). Example curves are shown as a function of probe detuning Δ_P in Fig. 3 for different control field detunings Δ_E. The EIT transmission window, as mentioned previously, has a finite bandwidth. This bandwidth is represented schematically by the shaded region in the uppermost curve of Fig. 3. Within this window the losses are low, because $\mathrm{Im}(\chi)$ is small, and the group velocity is low, because $\mathrm{Re}(\chi)$ has a very steep, linear slope. This is the signature behavior of slow-light schemes. For $\Delta_E=0$, the transparency occurs at $\Delta_P=0$ and is the region of low loss and widest linear dispersion. For nonzero Δ_E the transparency window is shifted to the point of two-photon resonance ($\Delta_P=\Delta_E$) and the EIT feature is somewhat distorted and asymmetric, though we still have a small region with low absorption and linear dispersion. For very large detuning ($\Delta_E \gg \gamma_{10}$) the absorption profile eventually goes over to a normal, lifetime-broadened Lorentzian peak at one-photon resonance ($\Delta_P=0$) and a very narrow peak just above the two-photon resonance.

Short pulses can have sufficiently broad bandwidths to exhibit effects of frequency-dependent absorption. An example of simulated transmission of a broad-bandwidth wave form through the system is presented in Fig. 4. In this calculation, we assumed $\Delta_E=0$ and a probe spectrum centered on $\Delta_P=0$. We used 20 Fourier components to represent an input square wave with a period of 40 μs, the higher-frequencies of which extend just beyond the lossless region – to $\pm2\pi\times1$ MHz. The output waveform is clearly delayed, but the sharp edges and the ripples, which form as a result of the higher-frequency components, have disappeared.

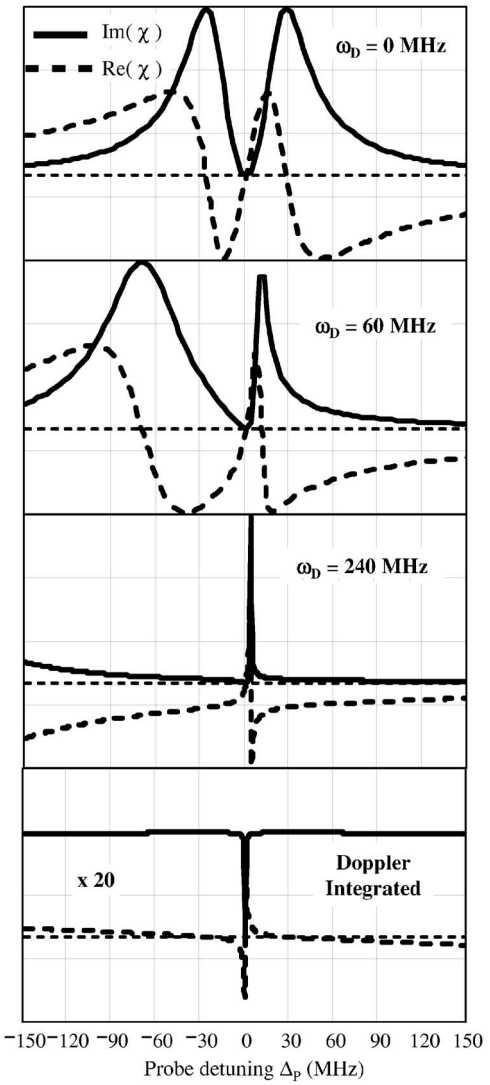

FIG. 5. Calculated susceptibility as a function of the probe frequency for different Doppler shifts ω_D.

Next we consider warm Rb vapor, in which Doppler shifts cannot be ignored. In this case, atoms moving with a velocity component v_z in the longitudinal direction z of the laser beam will appear to have different transition energies. In particular, the 0-1 transition and therefore both of the effective detunings of both lasers from resonance will be shifted by some amount $\omega_D(v_z)$. Figure 5 shows calculated real and imaginary values of the susceptibility as a function of the probe frequency for different Doppler shifts, keeping $\Delta_E=0$. Note the similarity to Fig. 3, except here the EIT transparency window stays fixed at $\Delta_P=0$. This is because the Dop-

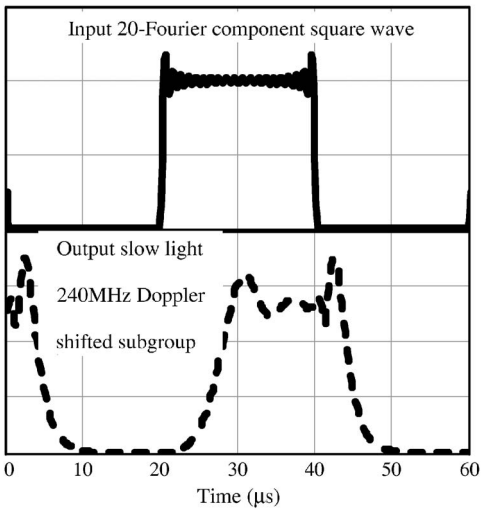

FIG. 6. Calculated slow light for atoms Doppler shifted by $\omega_D = 240$ MHz, $\Delta_E = 0$, and probe wave form centered about $\Delta_P = 0$. The pulse shape is greatly distorted by the strong EIT dispersion, but the high-frequency ripples demonstrate that at this Doppler shift the losses on the high-frequency components are smaller than for zero-velocity atoms.

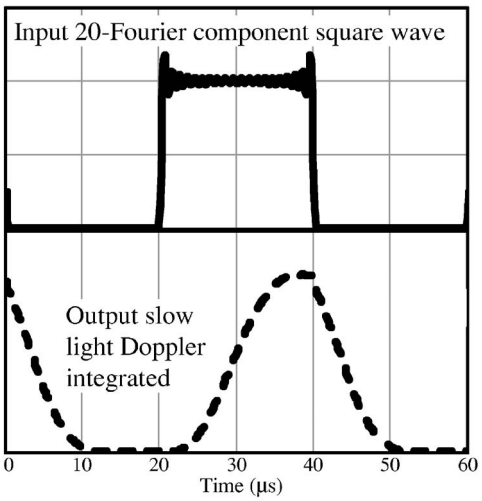

FIG. 7. Calculated slow light integrated over a Doppler profile.

pler shift acts to simultaneously shift both lasers and therefore affects the location of the one-photon resonance but not the two-photon resonance.

In analogy to what we observed for control field detunings Δ_E in Fig. 3, we see in Fig. 5 that for large ω_D the absorption spectra contain a narrow peak slightly detuned from the resonance, with the position of this peak depending on ω_D. Meanwhile, the background absorption near $\Delta_P = 0$ becomes much smaller. This results in higher overall absorption for the pulse but lower absorption of higher-frequency components. We also see a curvature in the slope of the real part of the susceptibility for various ω_D. Figure 6 shows a pulse propagated through a particular Doppler subgroup, detuned from the zero-velocity frequency by $\omega_D = 240$ MHz. Despite the distortion in the overall shape, the existence of rapid oscillations demonstrates the reduced loss of high-frequency components as compared to the zero-velocity case of Fig. 4.

The last plot in Fig. 5 shows the result of a full convolution of the susceptibility over all velocity components. The convolution was performed over a Maxwell distribution of velocities for an ensemble temperature of 65 °C, corresponding to the temperature of the vapor cell in the experiments, which has Doppler shifts over a width on the order of 300 MHz. As can be seen from the data, the effect of integrating over all Doppler shifts results in an EIT window that is approximately 50 times narrower than the zero-velocity case. Furthermore, there is now a large, flat absorption coefficient for light just outside this window, and the absorption here is less than the peak values of the zero-velocity case by a factor of about 20. This allows increased transmission of higher-frequency Fourier components.

Figure 7 shows a pulse propagating through an integrated Doppler profile. Most of the sharper features of a single detuning in Fig. 6 are gone, but the pulse undergoes a distinctive distortion simultaneously with the delay. Some remnants of higher frequencies are still present as we see a moderately sharp feature on the pulse turnoff. This is the same feature as that observed in the experiments. Interestingly, the shape of the Doppler-integrated profile (last panel of Fig. 5) in the limit of small detuning $\Delta_P \to 0$ is the same as the non-Doppler-broadened case (first panel). Thus the propagation of extremely narrow band pulses (like long Gaussians) can be modeled without inclusion of Doppler effects. However, the Doppler broadening restricts the region of validity of this treatment to a small region $\Delta_P < \Omega_E^2/\Delta\omega_D$, where $\Delta\omega_D$ is the Doppler width. Both the absorption and dispersion experienced by frequency components outside this region are quite affected by Doppler broadening, and this can strongly influence the resultant transmitted pulse shapes, as we observed here.

IV. SUMMARY

In conclusion, we observed unexpected pulse distortions of slowed, large-bandwidth pulses in warm Rb vapor. In particular, the transmitted pulses are not simply delayed pulses with higher-frequency components absorbed. Studying a model which takes into account one-photon detuning due to Doppler broadening isolates the origin of these distortions, and convolving over the full Doppler profile produces results which qualitatively match the experimental observations. In particular, this study isolates some important pulse distortion effects present in warm atomic vapors, not present in cold atom samples, which will be important in considering various applications of slow-light pulses.

ACKNOWLEDGMENT

This work is supported in part by the U.S. Office of Naval Research and Defense Advanced Research Projects Agency.

[1] Lene Vestergaard Hau, S. E. Harris, Zachary Dutton, and Cyrus H. Behroozi, Nature (London) **397**, 594 (1999).
[2] M. M. Kash *et al.*, Phys. Rev. Lett. **82**, 5229 (1999).
[3] D. Budker, D. F. Kimball, S. M. Rochester, and V. V. Yashchuk, Phys. Rev. Lett. **83**, 1767 (1999).
[4] Robert W. Boyd and Daniel J. Gauthier, Prog. Opt. **43**, 497 (2002).
[5] Jay R. Lowell and Enrique Parra, Proc. SPIE Int. Soc. Opt. Eng. **5735**, 80 (2005).
[6] Steve Harris, Phys. Today **50**(7), 36 (1997).
[7] M. O. Scully and M. S. Zubairy, *Quantum Optics* (Cambridge University Press, Cambridge, England, 1997).
[8] Andrew D. Greentree *et al.*, Phys. Rev. A **65**, 053802 (2002).
[9] Daniel A. Steck, http://steck.us/alkalidata, version 1.6, 14 October 2003 revision.